JCTC Journal of Chemical Theory and Computation

pubs.acs.org/JCTC Article

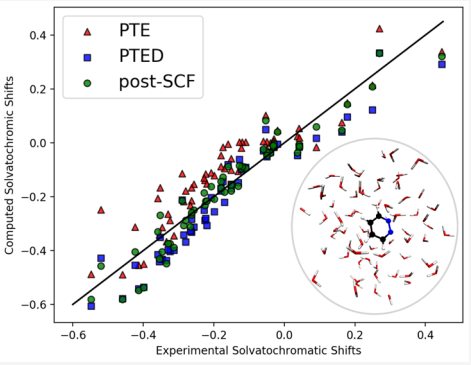
Comparison of Reaction Field Schemes for Coupling Continuum Solvation Models with Wave Function Methods for Excitation Energies

Sarah Karbalaei Khani,* Alireza Marefat Khah, and Christof Hättig

Cite This: *J. Chem. Theory Comput.* 2020, 16, 4554−4564 Read Online

ACCESS | Metrics & More | Article Recommendations | Supporting Information

ABSTRACT: We address in this work the question to which extend reaction field schemes for correlated wave function methods give accurate excitation energies and, at the same time, physically consistent potential energy surfaces. The performance of the perturbation on energy (PTE), perturbation on energy and density (PTED), and post-SCF reaction field schemes is compared for the algebraic diagrammatic construction through second-order, ADC(2), as electronic structure and the conductor-like screening model COSMO as solvation model. The conditions on reaction field schemes to give physically consistent potential energies surfaces are discussed at the example of 4-(*N*,*N*-dimethylamino)benzonitrile, which is used as a test case to assess the artifacts introduced by state-specific contributions to the effective Hamiltonian. To evaluate the accuracy for excitation energies, we use two benchmark sets with data in gas phase and solution for $\pi\pi^*$ and $n\pi^*$ electronic transitions. The experimental solvatochromic shifts are compared to the corresponding calculated values at the COSMO-ADC(2) level with the PTE scheme within the frozen solvent approximation, PTED with the linear response (LR) and corrected linear response (cLR) and post-SCF with LR schemes and with the approximate coupled-cluster singles and doubles method CC2 combined with COSMO in the post-SCF (LR) scheme. The PTE scheme gives at the COSMO-ADC(2) level less accurate solvent shifts than the PTED(LR), PTED(cLR), and post-SCF(LR) schemes. The most accurate prediction of solvatochromism is obtained with the post-SCF(LR) scheme. In most cases, PTED(cLR) performs similar to post-SCF, although its nonlinear perturbative correction causes problems for potential energy surfaces.



INTRODUCTION

There are various approaches to account for solvent effects on electronic excitation energies. Ab initio molecular dynamics (AIMD) approaches account for the atomistic and quantum mechanic nature of both solute and environment and the sampling over the thermally accessible configurations. They are computationally very demanding and thus essentially restricted to density functional theory (DFT) methods. Molecular dynamics with quantum mechanics/molecular mechanics (QM/MM) methods with polarizable or nonpolarizable force fields for the MM descriptions of the environment is an alternative that, although computationally more affordable than AIMD, is still very costly and requires the parametrization of the (polarizable) MM part which can make these approaches complicated to set up.[1] Implicit solvation models bypass the calculation of excitation energies for a large ensemble of solvent configurations by one or a few calculations within potentials that represent thermally averaged solvent environments. The embedded cluster reference interaction site model[2] (EC-RISM) belongs for example to this class of approaches. In particular continuum solvation models (CSMs) offer a cheap possibility to include the interactions with the bulk solvent which account often for the main effects of the environment on electronic transitions localized on a solute. Their great advantage is that the averaging over the environment configurations is included implicitly in the continuum description of the solvent. This makes the continuum models computationally efficient and easy to set up. These models can, however, not describe specific solute−solvent interactions like hydrogen bonds and also interactions beyond electrostatics such as dispersion and Pauli repulsion are difficult to include.[3]

The notion polarizable continuum model (PCM) is usually applied for CSMs that use the apparent surface charge (ASC) approach as boundary condition.[4] Different formulations of PCMs include dielectric PCM (D-PCM),[4] integral equation formalism PCM (IEF-PCM),[5] conductor-like PCM (C-PCM),[6] and conductor-like screening model COSMO.[7] C-

Received: March 30, 2020
Published: May 29, 2020



Downloaded via BOCHUM LIBRARIES on August 27, 2020 at 09:39:42 (UTC).
See https://pubs.acs.org/sharingguidelines for options on how to legitimately share published articles.

ACS Publications © 2020 American Chemical Society

https://dx.doi.org/10.1021/acs.jctc.0c00316
J. Chem. Theory Comput. 2020, 16, 4554−4564

PCM and COSMO are closely related and also perform similarly for electronic excitations. In the current study, COSMO is the solvent model of choice. It requires in addition to atomic radii for the definition of the cavity only two parameters that describe the macroscopic electrostatic properties of the solvent: the static dielectric constant ε and the optical dielectric constant $\varepsilon_{opt} = n^2$, where n stands for the index of refraction for a specific solvent.[7]

The description of solvent effects and its mutual interaction with the solute on the solute's wave function without having a wave function for the total system is the subject of the self-consistent reaction field (SCRF) theory.[8] In CSMs, including COSMO, the polarization of the solvent by the solute's nuclear and electronic charge distribution is described by apparent surface charges on the cavity surface. The mutual solute−solvent polarization with the solvent in equilibrium with the solute in its electronic ground state can for the self-consistent field (SCF) methods, that is, Hartree−Fock (HF) or DFT, be determined within the SCF cycles fully self-consistently without much overhead. For electronic excitations, when sudden transitions between two electronic states with different charge distributions are considered, the situation is more complicated. In general, to determine excitation energies, one can use either (i) a state-specific (SS) approach by solving approximately the electronic Schrödinger equation for the ground and the excited state and calculating the excitation energy as the difference of the total energies of the states or (ii) linear response (LR) theory, where the excitation energies are determined as eigenvalues of an electronic Hessian or Jacobian.

The two approaches are equivalent for linear variational methods, for example, configuration interaction methods in vacuum, but become inequivalent within SCRF theory, for example for molecules in solution, and then take different contributions into the account.[9,10] The SS approach includes the change of solvent polarization (the reaction field) due to the change in the solute's charge distribution upon excitation. The LR approach, on the other hand, accounts for the excitonic coupling of the solute's transition density to the fast optical polarizability of the environment, associated with the relaxation of electrons, but does not account for the change in the reaction field induced by the difference between the excited-state and the ground-state electron densities.[11,12] To overcome this intrinsic limit, Caricato et al. introduced the corrected linear response (cLR) approach[13] which adds, on top of the LR results, a perturbative correction to include the relaxation of the reaction field to the change of the solute's charge density upon excitation.[14−16]

Also, if used within the SCRF theory, the SS approach gives nonorthogonal wave functions, while the LR approach conserves the orthogonality of the wave functions. As a consequence, potential energy surfaces (PESs) obtained with the SS approach become physically inconsistent at avoided crossings and conical intersections while the LR approach gives consistent excited-state PESs. The perturbative correction of the cLR approach leads again to similar problems for PESs as the SS approach.

For post-SCF correlation methods, another level of complexity arises for different schemes to include the correlation effects in the determination of the reaction field as the perturbation on energy (PTE),[17] the perturbation on density (PTD),[17] the PTE(S) and PTES (where "S" stands for singles),[18] the post-SCF,[19] and the perturbation theory with self-consistent energy and density (PTED).[12,17] These schemes were initially introduced for ground-state energies with correlated wave function methods, in particular Møller−Plesset perturbation theory (MPn). For excitation energies, they have to be combined with either the SS or LR approaches. As pointed out above, the physically correct description of PESs in the regions of (avoided) crossings imposes restrictions on the approximations that can be used for the reaction field scheme. This is important for all applications that involve excited state PESs as, for example, studies of relaxation processes after photoexcitation and, technically, in particular for the development of analytic excited-state gradients. First implementations of such gradients for a CSM and a QM/MM approach with a polarizable MM environment and the algebraic diagrammatic construction through second-order, ADC(2), as a correlated wave function method were recently presented for COSMO-ADC(2) and PE-ADC(2) (where "PE" stands for the polarizable embedding) using the LR approach with the post-SCF reaction field scheme.[20,21] This was to some extend motivated by the simplicity and computational efficiency of this reaction field scheme.

The purpose of the present contribution is to evaluate and compare the appropriateness for PESs and accuracy of excitation energies of the above-mentioned reaction field schemes for correlated wave function methods. To this end, we used ADC(2) and, for vertical excitation energies, in addition the approximate coupled-cluster singles and doubles model CC2 as QM methods with the COSMO continuum solvation model.

A benchmark study for different perturbative reaction field schemes for vertical excitation energies that used ADC(2) together with PCM was reported earlier by Mewes et al.[22] They used a narrow set of organic molecules mostly having very close chemical structures and only $\pi\pi^*$ electronic transitions. In the present contribution, we, therefore, used also a second test set comprised of more diverse molecular systems with a mixture of $\pi\pi^*$ and $n\pi^*$ transitions.

REACTION FIELD SCHEMES

In CSMs, the solute is in a molecular-shaped cavity within the dielectric medium that represents the solvent, and the mutual solute−solvent interactions induce charges on the cavity surface. The cavity is usually composed of triangular segments, and the surface charges are approximated by point charges at the centers of the segments. For COSMO, the apparent surface charge Q_κ on the cavity segment κ is obtained as[7]

$$Q_\kappa = -f(\varepsilon) \sum_\lambda [\mathcal{A}^{-1}]_{\kappa\lambda} V_\lambda \tag{1}$$

where V_λ is the electric potential at the center of the segment λ due to the charge distribution in the solute. $\mathcal{A}_{\kappa\lambda}$ is the COSMO kernel describing the interaction between surface segments, and $f(\varepsilon)$ is a scaling factor that depends on the dielectric constant ε which in principle depends on the frequency with which V_λ varies. The definition of $\mathcal{A}$ and $f(\varepsilon)$ are given in ref 12, and the cavity construction is described in ref 23.

The coupling of the continuum solvent model with the QM description of the solute leads to the definition of an effective Hamiltonian and a nonlinear Schrödinger equation

$$\hat{H}^{\text{eff}}|\Psi\rangle = \left\{\hat{H}^{\text{vac}} + \sum_\kappa Q_\kappa \cdot \hat{V}_\kappa\right\}|\Psi\rangle = E|\Psi\rangle \tag{2}$$

https://dx.doi.org/10.1021/acs.jctc.0c00316
J. Chem. Theory Comput. 2020, 16, 4554−4564

In this equation, $\hat{H}^{\mathrm{vac}}$ is the vacuum Hamiltonian and $\hat{V}_\kappa$ the Coulomb potential due to a unit charge in the center of segment κ. The free energy of the solute which includes in addition to the solute's internal energy and the interaction with the solvent also the work for inducing the surface charges is

$$G^{\mathrm{solv}} = \langle\Psi|\hat{H}^{\mathrm{vac}} + \frac{1}{2}\sum_\kappa Q_\kappa \cdot \hat{V}_\kappa|\Psi\rangle \tag{3}$$

In variational quantum chemistry methods the ground-state wave function is determined by minimizing G^{solv} for the given wave function ansatz. For Hartree−Fock, this leads to expressions which are analogous to the vacuum case, just with the vacuum Fock operator augmented by a reaction field (RF) contribution $\hat{G}^{\mathrm{HF}}$

$$\hat{F}^{\mathrm{pol}} = \hat{F} + \hat{G}^{\mathrm{HF}} \tag{4}$$

$$\hat{G}^{\mathrm{HF}} = \sum_\kappa Q_\kappa^{\mathrm{HF}} \cdot \hat{V}_\kappa \tag{5}$$

where $\hat{Q}_\kappa^{\mathrm{HF}}$ are the surfaces charges computed from the HF density. The polarized canonical orbitals and orbital energies are now obtained as eigenvalues and eigenvectors of $\hat{F}^{\mathrm{pol}}$. Analogous equations are obtained for Kohn−Sham DFT. In the following, we briefly sketch the reaction field schemes for electronic ground and excited states used in this study.

Ground State. A straightforward possibility to include the essential solvent contributions in correlated post-SCF methods for ground-state energies is the PTE reaction field scheme. In PTE calculations, the Hartree−Fock RF potential $\hat{G}^{\mathrm{HF}}$ is used without further alteration in post-HF calculations, for example, Møller−Plesset perturbation theory (MPn) or any other correlation method. This approximation neglects any correlation contributions to the reaction field. While this is consistent with MP2,[24] for correlation methods beyond MP2, it is an additional approximation. In the full configuration interaction (FCI), PTE calculations do not converge to the variational minimum of G^{solv}, eq 3. In the PTED scheme, the RF potential and the density of the post-SCF calculation are determined fully self-consistently. It is formally the complete RF scheme and gives results that converge in the FCI or FCC limit to the variational minimization of G^{solv}. A disadvantage of the PTED scheme is that the macro iterations over the SCF and post-SCF calculations can cause problems in combination with the response theory, for example, at the coupled cluster level. The dependence of the effective Hamiltonian on the charge density of the target state can, for example, lead to root flipping problems.

The post-SCF reaction field scheme[19] was devised to avoid the computational costs that arise from the macro-iterations of the PTED approach. In this RF scheme, a post-SCF contribution to the RF potential is calculated from the correlation contribution to the wave function, which is included in the equations for the post-SCF wave function parameters, but not coupled back into the Hartree−Fock calculation. It converges to the correct FCI limit and is fully compatible with the response theory. The PTES and PTE(S) schemes[18] are closely related approximations proposed for CCSD that compute the post-SCF contribution to the RF potential only from the single amplitudes.

Excited State. For studying excited states in solution, the simplest and computationally cheapest approach is to apply the PTE scheme in combination with the frozen solvent approximation[25] for the excitation energy, that is, to keep the surface charges, calculated at the COSMO-HF level, fixed during the whole post-HF correlation and excitation energy calculations. In this scheme, the solute−solvent interactions enter in the post-HF calculations only as a static one-electron potential, usually included by replacing the vacuum Fock operator $\hat{F}$ by $\hat{F}^{\mathrm{pol}}$. At the ADC(2) level, excitation energies ω_i are obtained as eigenvalues of a secular matrix[26]

$$\begin{pmatrix} \mathbf{A}_{\mu_1\nu_1} & \mathbf{A}_{\mu_1\nu_2} \\ \mathbf{A}_{\mu_2\nu_1} & \mathbf{A}_{\mu_2\nu_2} \end{pmatrix} \begin{pmatrix} \mathbf{E}^i_{\nu_1} \\ \mathbf{E}^i_{\nu_2} \end{pmatrix} = \omega_i \begin{pmatrix} \mathbf{E}^i_{\mu_1} \\ \mathbf{E}^i_{\mu_2} \end{pmatrix} \tag{6}$$

where the indices μ_1, ν_1 and μ_2, ν_2 run over singly and doubly excited Slater determinants or configuration state functions, respectively. At the COSMO-ADC(2) PTE level, explicit reaction field contributions enter only in the singles−singles and the double−doubles block of the secular matrix

$$\mathbf{A}^{\mathrm{pol}}_{\mu_1,\nu_1} = \langle\mu_1|\hat{G}^{\mathrm{HF}}|\mathrm{HF}\rangle \tag{7}$$

$$\mathbf{A}^{\mathrm{pol}}_{\mu_2,\nu_2} = \langle\mu_2|[\hat{G}^{\mathrm{HF}}, \tau_{\nu_2}]|\mathrm{HF}\rangle \tag{8}$$

and are usually included through the Fock matrix.

For reaction field schemes that go beyond the frozen solvent approximation, the different time scales for the response of the electronic and nuclear (or orientational) motions in the solvent comes into play. When the solute charge density undergoes a fast change, as it is the case for vertical electronic excitations, only the solvent's electrons are assumed to be fast enough to respond while the orientation of the solvent molecules remains for a short time scale in its initial configuration. To describe this nonequilibrium situation, the response of the solvent is split into its slow (nuclear) and fast (optical or electronic) contributions. The latter is determined from the refractive index n of the solvent by using it for the fast response contributions to the surface charges $f(n^2)$ as a scaling factor in eq 1.[27]

The main effects beyond the frozen solvent approximation are the interaction of the transition density of the solute with the dynamic response of the reaction field, the so-called excitonic coupling, and the interaction of the density change upon excitation with the solvent polarization.[11,12,28] The former effect is particularly crucial for bright electronic transitions with large transition dipole moments. As mentioned in the introduction, the LR approach accounts for the excitonic coupling. However, for excitations associated with a significant change in the solute's electron density, such as excitations with a charge-transfer character, the response of the solvent polarization to the change of charge density differences upon excitation is important. It is included (self-consistently) only by the SS, and not by the LR approach. The cLR approach accounts for the former effect by a noniterative perturbative correction.

Lunkenheimer and Köhn's implementation of the PTED scheme for excitation energies and absorption spectra with COSMO-ADC(2)[12] belongs to the category of cLR approaches and is probably the physically most complete RF scheme implemented at the ADC(2) level. It starts with a COSMO-MP2 PTED calculation where the ground-state RF potential and the orbital-relaxed MP2 density are determined self-consistently in a macro iteration loop over the HF and the MP2 ground-state calculations using $f(\varepsilon)$ as the scaling factor.

https://dx.doi.org/10.1021/acs.jctc.0c00316
J. Chem. Theory Comput. 2020, 16, 4554−4564

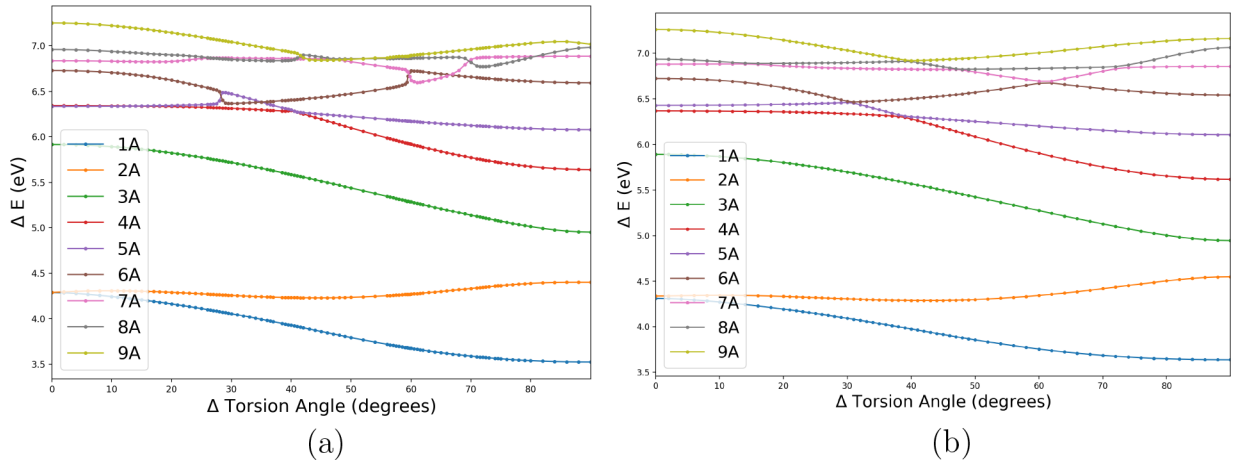


Figure 1. Potential energy curves for the lowest states of DMABN in acetonitrile solution with COSMO-ADC(2)/def2-TZVPP using (a) the PTED with corrected linear response approach and (b) the post-SCF with linear response approach. In both cases the RF has been equilibrated for the ground state (for details see the text).

Initial excitation energies are then calculated using the LR approach. Explicit RF contributions enter again only in the singles−singles and the doubles−doubles block:

$$\mathbf{A}^{\mathrm{pol}}_{\mu_1,\nu_1} = \langle \mu_1 | [\hat{G}^{\mathrm{MP2}}, \tau_{\nu_1}] + \hat{G}^{\nu_1} | \mathrm{HF} \rangle + \frac{1}{2}(\langle \mu_1 | [\hat{G}^{\nu_1}, \hat{T}_2] | \mathrm{HF} \rangle + \langle \nu_1 | [\hat{G}^{\mu_1}, \hat{T}_2] | \mathrm{HF} \rangle) \quad (9)$$

$$\mathbf{A}^{\mathrm{pol}}_{\mu_2,\nu_2} = \langle \mu_2 | [\hat{G}^{\mathrm{MP2}}, \tau_{\nu_2}] | \mathrm{HF} \rangle \quad (10)$$

$\hat{G}^{\mathrm{MP2}}$ is the COSMO-MP2 PTED ground-state reaction field potential, which is again included through the Fock operator. The operator $\hat{G}^{\nu_1}$, accounting for the response contributions, is defined as

$$\hat{G}^{\nu_1} = -f(n^2) \sum_{\kappa\lambda} \hat{V}_\kappa [\mathcal{A}^{-1}]_{\kappa\lambda} \langle \mathrm{HF} | [\hat{V}_\lambda, \tau_{\nu_1}] | \mathrm{HF} \rangle \quad (11)$$

and computed with the scaling factor for optical frequencies. For the cLR approach, a perturbative correction for the response of the reaction field to the change in the solute's charge density upon excitation is added to the eigenvalue of the secular matrix **A** as described in ref 12

$$\Delta G_i = \omega_i - f(n^2)\frac{1}{2} \sum_{\kappa\lambda} (V^{(i)}_\kappa - V^{\mathrm{MP2}}_\kappa)[\mathcal{A}^{-1}]_{\kappa\lambda} (V^{(i)}_\lambda - V^{\mathrm{MP2}}_\lambda) \quad (12)$$

where V^{MP2}_κ is the potential on the surface segment κ because of the orbital-relaxed MP2 ground-state charge density of the solute. $V^{(i)}_\kappa$ is the respective potential for state i, calculated with the orbital-relaxed ADC(2) excited state density.[12]

In the post-SCF scheme, the ground-state reaction field is first determined self-consistently at the COSMO-HF level. In the subsequent correlation treatment, the correlation effect to the RF is calculated from the correlation contribution to the (unrelaxed) density and included in the equations for the ground-state wave function parameters but not coupled back into the Hartree−Fock calculation. Excitation energies are then calculated by the LR approach. For the second-order methods ADC(2) and CC2 we neglect in the post-SCF scheme in addition the contributions from doubles amplitudes in the unrelaxed densities since they introduce contributions beyond second order. With this approximation, for ADC(2), the ground state becomes identical with COSMO-MP2 PTE. Without state specific corrections, the polarization contributions to the secular matrix elements of the COSMO-ADC(2) post-SCF are

$$\mathbf{A}^{\mathrm{pol}}_{\mu_1,\nu_1} = \langle \mu_1 | [\hat{G}^{\mathrm{pol,HF}}, \tau_{\nu_1}] + \hat{G}^{\nu_1} | \mathrm{HF} \rangle \quad (13)$$

$$\mathbf{A}^{\mathrm{pol}}_{\mu_2,\nu_2} = \langle \mu_2 | [\hat{G}^{\mathrm{pol,HF}}, \tau_{\nu_2}] | \mathrm{HF} \rangle \quad (14)$$

where $\hat{G}^{\mathrm{pol,HF}}$ accounts for the polarization contributions induced by the ground-state Hartree−Fock density and is usually included via the Fock matrix.

Excited State PES. As already pointed out in the introduction, the state-specific contributions in the SS and the perturbative correction for the cLR approach cause problems for excited-state potential energy surfaces. They lead to unphysical shapes in the vicinity of conical intersections and avoided crossings. Furthermore, the macro iterations for the self-consistent determination of the correlated ground-state reaction field in the PTED schemes make the calculation of gradients for such schemes challenging and potentially numerically unstable.

To demonstrate these problems, we scanned the potential energy surface for the lowest states of 4-(*N*,*N*-dimethylamino)-benzonitrile (DMABN) in acetonitrile solution along the phenyl-amino torsion angle with all other internal coordinates kept fixed at their values in the ground-state COSMO-MP2 PTE geometry. Figure 1 depicts the results obtained in the def2-TZVPP basis[29] at the COSMO-ADC(2) level using the PTED(cLR) and post-SCF(LR) approaches. As is evident from the results, in the cLR approach the perturbative state-specific corrections, which depend on the excited-state densities, lead to unphysical shapes of the PES around avoided crossings regions for the forth to the ninth excited states (cmp. Figure 1a). Instead of avoided crossings one obtains unphysical multiple crossings. The post-SCF scheme with the LR approach has been designed such that it does include neither perturbative corrections nor variational state-specific contributions and does not require macro-iterations over SCF and post-SCF parts, which would hamper tight convergence. It gives smooth PES with physically correct shapes at avoided crossings as seen in Figure 1b.

https://dx.doi.org/10.1021/acs.jctc.0c00316
J. Chem. Theory Comput. 2020, 16, 4554−4564

COMPUTATIONAL DETAILS

Test set I is taken from a benchmark study by Mewes et al.[22] with reference data for experimental band maxima in the gas phase and nonprotic solvents for nitrobenzene[22] and meta- and para-substituted methyl-, chloro-, amino-, and methoxy-nitrobenzene,[30] meta- and para-methoxy-nitroaniline,[31] benzofuran, cumarin, and pyridine.[22] Given that test set I consists of molecules that are structurally very close, we decided to collect a second test set (II) with more diverse chromophores. The reference data for test set II are again experimental band maxima in the gas phase and solution, and the test is comprised of lowest excitations for the molecules acrolein,[32−36] azobenzene,[37,38] benzaldehyde,[14,39−41] 4-(*N*,*N*-dimethylamino)benzonitrile (DMABN),[42−44] pyridazine,[45−50] anthracene,[51,52] adenine,[53−55] guanine,[55,56] uracile,[14,55] indole,[48,57,58] xanthone,[59,60] and acetone.[61] This test set also includes data for solution in the protic solvents water and ethanol. Furthermore, to avoid a biased analysis toward $\pi\pi^*$ excitations, the two test sets (one with 35 $\pi\pi^*$ transitions and the other one with a mixture of 15 $\pi\pi^*$ and 7 $n\pi^*$ states) are analyzed separately.

Optimized geometries for the ground state in the gas phase, as well as in solution, were obtained at the MP2/def2-TZVP level of theory[29] in combination with the COSMO solvation model within the PTE scheme as implemented in TURBOMOLE.[62] For the ADC(2) and CC2 calculations we used the resolution-of-the-identity (RI) approximation with the optimized def2-TZVP auxiliary basis set from ref 63. The frozen core approximation was applied to all non-hydrogen atoms: for all C, O, and N atoms the $1s^2$ electrons were kept frozen and for chlorine, in addition, all electrons in the $2s^22p^6$ shell. The solvatochromic shifts at the COSMO-ADC(2)/def2-TZVP level within the PTE, PTED(LR), and PTED(cLR) reaction field schemes were computed with release V7.3 of TURBOMOLE[62] and for the post-SCF scheme with a local development version of the package.[20,64] For consistency, we have not included any out-lying charge corrections in the COSMO calculations. We tested its effect for PTED with the cLR scheme. For test set I, its effect on the excitation energies was only −0.002 ± 0.001 eV and for test II only −0.0009 ± 0.0006 eV. Compared to other intrinsic errors of COSMO and the reaction field schemes investigated here, the outlying charge correction is completely negligible. The solvent parameters are given in Table 1. For the cavity construction

Table 1. Dielectric Constants for Different Solvents Used in the Calculations

solvent	static dielectric ε	optical dielectric n^2
hexane (Hex)	1.89	1.88
cyclohexane (cyHex)	2.03	2.02
diethyl ether (Et_2O)	4.32	1.83
ethanol (EtOH)	24.6	1.85
acetonitrile (MeCN)	36.7	1.81
water (H_2O)	80.4	1.78

the solvent accessible surface (SAS) approach[7,23,65,66] is used for all solvents, with atomic radii (r_O = 1.72 Å, r_N = 1.83 Å, r_C = 2.00 Å, and r_H = 1.30 Å) and the solvent radius (r_{solv} = 1.30 Å), chosen according to the recommendations in refs 7 and 65.

RESULTS AND DISCUSSION

First Data Set. The solvent shifts obtained for test set I in hexane, cyclohexane, diethyl ether, and acetonitrile with COSMO-ADC(2) and the PTE, PTED(LR), PTED(cLR) and post-SCF(LR) RF schemes are compared to the respective experimental values in Figure 2. As noted in ref 22, solvent shifts for cumarin, benzofuran, pyridine, and nitrobenzene, with weak electrostatic interactions with the solvent, are both computationally and experimentally low, especially for pyridine and the lowest bright states of cumarin and benzofuran, while their second bright states show larger shifts. The weak solute−solvent interactions for these states come with too small solvent shifts in the PTE approach. Also for the cases with larger, mostly negative, solvent shifts the PTE scheme systematically underestimates the absolute values of the experimental solvent shifts. This is a consequence of the fact that the contributions from the excitonic coupling and the response of the RF to the density change upon excitation, which are neglected in the PTE approach, are both negative.

For the PTED(cLR) and post-SCF(LR) RF schemes, we observe that for nonpolar (Hex and cyHex) and intermediate-polar solvents (Et_2O) the solvent shifts computed with these two approaches differ more than for polar solvents (MeCN). Both schemes have a tendency to overestimate the magnitude of negative (red-shifting) solvent shifts. For the nonpolar solvents, the red shifts for the post-SCF scheme are smaller than for the PTED(cLR) scheme and larger than for the PTED(LR) and, thus, are at the same time for most cases closer to the respective experimental values. On the other hand, for MeCN, the solvent red shifts computed with post-SCF and PTED(cLR) approaches are closer. This means that for polar solvents the additional contributions from correlation effects on the ground-state RF and the excitonic coupling, that is, the difference between the post-SCF(LR) and the PTED(LR) results, at least for molecules in this test set, canceled to large extent by the response of the RF to the density change upon excitation, the difference between PTED(LR) and PTED(cLR). For nonpolar solvents, where the correlation effects to the ground-state RF (i.e., to the frozen solvent contributions) are tiny, this is not the case.

A statistical analysis of the errors for the solvatochromic shifts obtained at the COSMO-ADC(2) level with the PTE, PTED(LR), PTED(cLR), and post-SCF reaction field schemes and for COSMO−CC2 with the post-SCF RF is shown in Figure 3. Here, we included CC2 to get an impression on how transferable the trends seen for ADC(2) are to other correlated second-order methods. At the COSMO-ADC(2) level, the best agreement with the experimental solvent shifts is obtained with the post-SCF RF scheme, although the mean absolute error (MAE) is for all four schemes and all four solvents bellow 110 meV. From the very simple PTE to the formally most complete PTED(cLR) RF scheme, the accuracy of the computed shifts improves for test set I in particular for Hex, cyHex, and Et_2O solutions. At the same time, the mean absolute deviations for the solvent shifts for these three solvents with the post-SCF scheme is smaller than for PTED(LR) and PTED(cLR) with MAEs of 23 meV, 23 and 33 meV for Hex, cyHex, and Et_2O. Also, the perturbative state-specific correction which is added to the PTED(LR) results to arrive at the final PTED(cLR) does, at least for this test set, not improve the results. In particular the discrepancy from the experimental solvent shifts increases for the polar acetonitrile

https://dx.doi.org/10.1021/acs.jctc.0c00316
J. Chem. Theory Comput. 2020, 16, 4554−4564

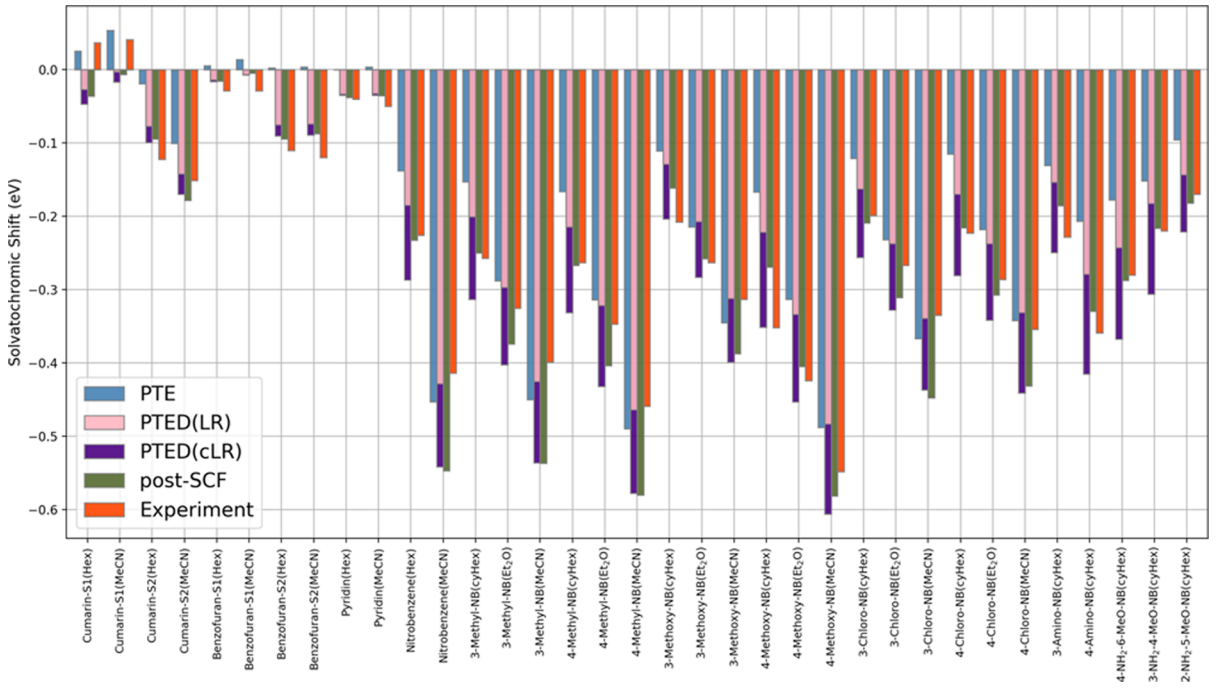


Figure 2. Experimental and computational solvent shifts at the COSMO-ADC(2)/def2-TZVP level with the PTE, PTED(LR), PTED(cLR), and post-SCF RF schemes. Solvents are in parentheses.

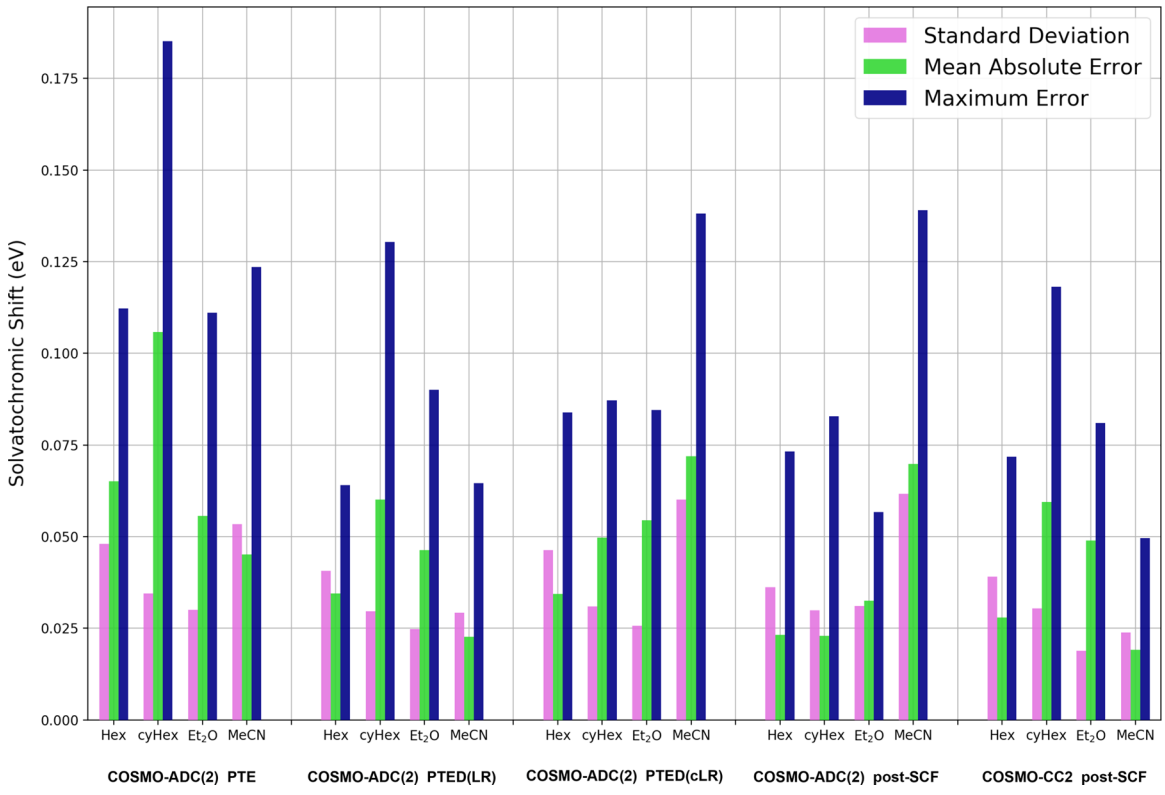


Figure 3. Statistical errors for the difference between calculated and experimental solvatochromic shifts at the COSMO-ADC(2)/def2-TZVP level with the PTE, PTED(LR), PTED(cLR), and post-SCF scheme and for COSMO−CC2/def2-TZVP with the post-SCF scheme.

as solvent. Because of error compensation, the shifts obtained for MeCN solvent with COSMO-ADC(2) PTE show a better agreement with the experimental results (MAE = 45 meV and max. error = 123 meV) than COSMO-ADC(2) with the more advanced PTED(cLR) and post-SCF schemes (MAEs of 72 and 70 meV and max. errors of 138 and 139 meV, respectively). Interestingly, the solvent shifts obtained for MeCN solutions with the post-SCF scheme in combination with COSMO−CC2 are for this test set significantly more accurate. This indicates that at least for nitrobenzene and its derivatives the ground-state singles amplitudes, that are included for CC2 but not for ADC(2), are important for

https://dx.doi.org/10.1021/acs.jctc.0c00316
J. Chem. Theory Comput. 2020, 16, 4554−4564

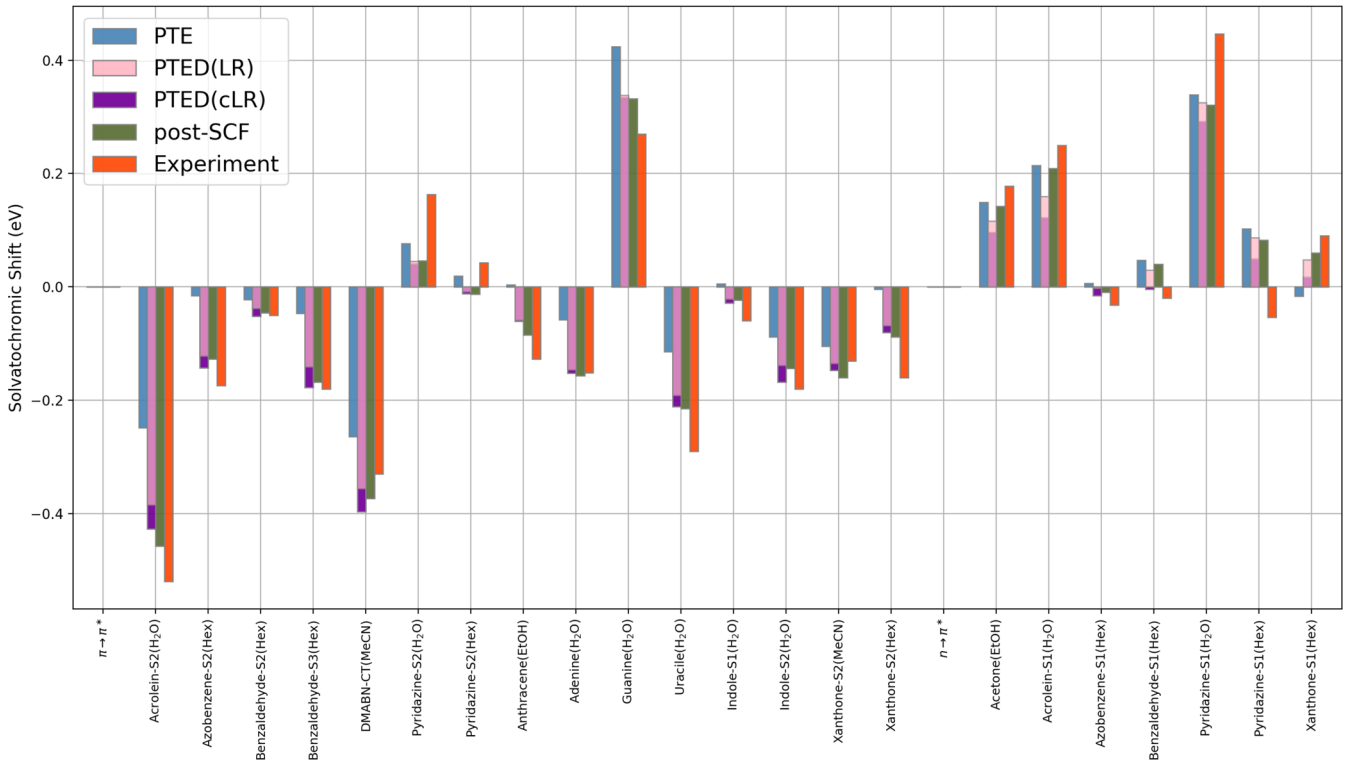


Figure 4. Experimental and computed solvent shifts at the COSMO-ADC(2)/def2-TZVP level with the PTE, PTED(LR), PTED(cLR), and post-SCF RF schemes.

accurate solvent shifts in polar solvents. However, in general, the performance of COSMO−CC2 and COSMO-ADC(2) with the post-SCF scheme are similar, so that one can expect that the trends found for the different reaction field approaches with ADC(2) are transferable to other correlated second-order methods.

Second Data Set. Test set I focused on excited states with $\pi\pi^*$ character in a relative narrow set of chromophores, mostly nitrobenzenes. Therefore, we collected data for a second test set (II) that includes more diverse molecular structures and excited states and includes data for the protic solvents water and ethanol. It is comprised of 12 different molecules with $\pi\pi^*$ and $n\pi^*$ transitions in the solvents water (H_2O), Hex, MeCN, and ethanol (EtOH) in total data for 22 solvent shifts. We computed the solvent shifts again at the COSMO-ADC(2)/def2-TZVP level with the RF schemes PTE, PTED(LR), PTED(cLR), and post-SCF. In Figure 4, the results for the second data set are compared to the corresponding experimental values. An inspection of Figure 4 reveals that the performance of post-SCF (mean error (ME) 13.3 meV and MAE 46.7 meV), PTED(LR) (ME 29.8 meV and MAE 56.4 meV), and PTED(cLR) (ME 13.0 meV and MAE 48.1 meV) are very close, if we only consider the $\pi\pi^*$ transitions. For the $\pi\pi^*$ transitions, the solvent shifts are in most cases negative, and the PTE scheme gives too small red or too large blue shifts, probably mainly because of the neglect of excitonic coupling of the transition densities to the optical polarizability of the solvent.

The blue solvent shifts observed for the $n\pi^*$ transitions in test set II in both experiment and theory are related to the changes in the solute's charge density that come with the transition of an electron for a lone pair into the π-system and is dominated by the frozen solvent contribution. For the protic solvents, water and ethanol, hydrogen bonds between OH groups of the solvent and the lone pair involved in the $n\pi^*$ transition are expected to contribute significantly to the solvent shift. This interaction between the positively polarized H atoms in the OH groups of the solvent with electrons in the n orbital of the solute leads to the stabilization of the ground state relative to the excited state at the time of the excitation process. The shifts for $n\pi^*$ states predicted by the post-SCF scheme with an ME of −2.2 meV and an MAE of 64.5 meV and PTED(LR) with an ME of −13.8 meV and an MAE of 76.5 meV have relatively small errors, while the PTED(cLR) scheme has on average larger deviations from the experimental results with an ME − 43.1 meV and an MAE of 81.6 meV. Again, the PTED(cLR) scheme with COSMO-ADC(2) overestimates the red-shifting relative to the blue-shifting contributions to these excitation energies in solution. The values of the ME and MAE for the PTE scheme for this type of transitions are with, respectively, −2.7 and 76.9 meV close to the post-SCF values, which is related to the relatively small transition dipole moments of the $n\pi^*$ states. For test II, the perturbative state-specific corrections are for all cases small, essentially negligible compared to the intrinsic errors of ADC(2) and the comparison of computed shifts for vertical excitation energies with experimental shifts of band maxima.

For pyridazine, which has a comparatively large deviation of the COSMO-ADC(2) results from experiment, one can expect that the hydrogen bonding interactions between the solute and the solvent, which are not well described by continuum models, need to be included to obtain accurate results at least by adding some explicit solvent molecules in the quantum mechanically treated system. To investigate this, we performed a classical molecular dynamics (MD) simulation with the CHARMM36 force field[67] (CGenFF) to evaluate how many

https://dx.doi.org/10.1021/acs.jctc.0c00316
J. Chem. Theory Comput. 2020, 16, 4554−4564

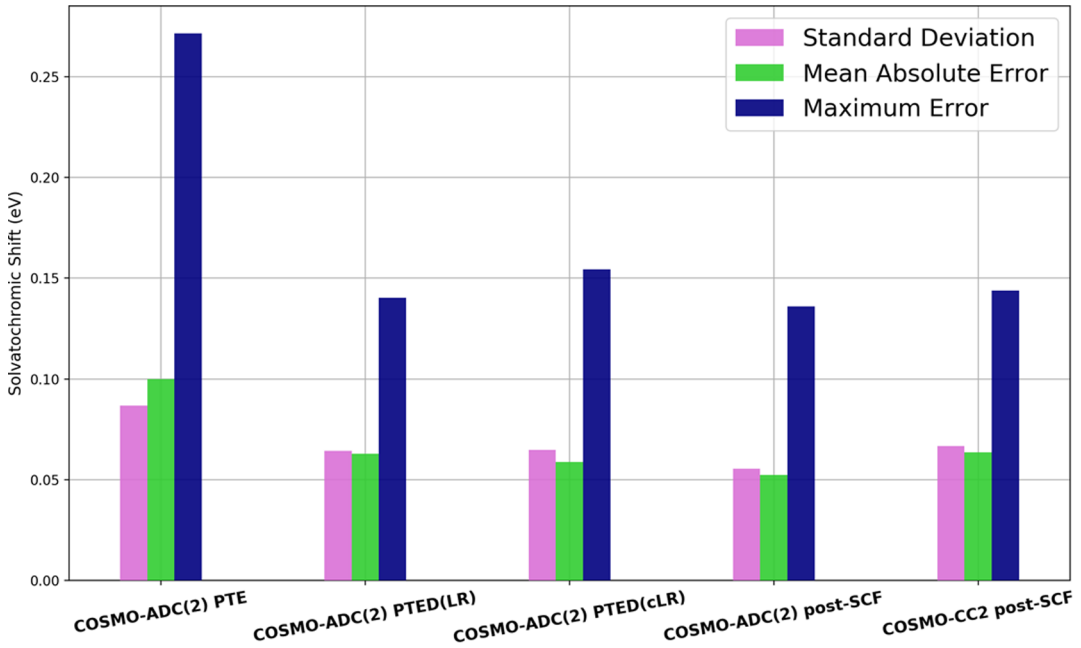


Figure 5. Statistical evaluation for the deviations between calculated and experimental solvatochromic shifts at the COSMO-ADC(2)/def2-TZVP level with the PTE, PTED(LR), PTED(cLR), and post-SCF schemes and the COSMO−CC2/def2-TZVP level with the post-SCF scheme. For the S_1, state of pyridazine in H_2O, the pure COSMO results without H_2O molecule in the QM system were included in the analysis.

Table 2. Analysis of the Various Reaction Field Contributions to Solvent Shifts[a]

mol.	state	exp.	PTE	PTED(FrozSol)	PTED(LR)	PTED(cLR)	post-SCF
NB	S4($\pi\pi^*$)	−0.41	−0.45	−0.35	−0.43	−0.54	−0.55
AC	S1($n\pi^*$)	0.25	0.21	0.17	0.16	0.12	0.21
	S2($\pi\pi^*$)	−0.52	−0.25	−0.21	−0.39	−0.43	−0.46

[a]Excitation energy shifts (eV) are computed at the COSMO-ADC(2)/def2-TZVP level. NB stands for nitrobenzene in acetonitrile solution and AC stands for acrolein in aqueous solution.

water molecules of the first solvation shell are making hydrogen bonds particularly with the nitrogen atoms of pyridazine. Trajectory analysis reveals that pyridazine is most of the time only hydrogen bonded to one water molecule. Including this water molecule in the QM subsystem for the COSMO-ADC(2) calculations improves the computed value for the solvatochromic shift for the $n\pi^*$ state significantly. It decreases the experiment-theory gap for post-SCF from 126.3 to 20.7 meV, for PTED(cLR) from 154.3 to 45.6 meV and for PTE from 107.8 to 5.1 meV (see Supporting Information for computational details of the classical MD simulation).

Figure 5 summarizes the statistical evaluation for both the $\pi\pi^*$ and $n\pi^*$ transitions. The PTE scheme gives for test set II significantly less accurate results than the PTED(LR), PTED(cLR), and the post-SCF scheme. Between the latter three, we observe for the test set II overall only minor differences in the performance, which are not significant considering the small size of the test set. Also between the ADC(2) and CC2 results for the solvent shifts within the post-SCF scheme, we see for test set II not such large differences as for test set I. They are, thus, most likely a peculiarity of the transitions included for the nitrobenzenes, which have for some substituents a partial charge-transfer character.

To study the effect of the various reaction field contributions in the PTED(cLR) scheme, electronic excitation energies of two molecules selected from both test sets have been compiled in Table 2 and compared to the post-SCF scheme. The contribution from the ground-state Hartree−Fock reaction field (PTE) is included in all schemes. It can be negative or positive, depending on whether its interaction with the change of the charge density upon excitation is, respectively, attractive or repulsive. The replacement of ground state HF RF with that from MP2 but still using the frozen solvent approximation, in Table 2 denoted as PTED(FrozSol), decreases the magnitude of the solvatochromic shifts. This can probably be interpreted such that the correlated density is more diffused than the noncorrelated Hartree−Fock density and thus interacts less strongly with the difference density between ground and excited state. The linear contribution and the perturbative state-specific corrections are both always negative. For the $\pi\pi^*$ transitions, where the frozen solvent contribution is negative, and thus, its correlation contribution positive, the difference between PTED(FrozSol) and PTE cancels almost completely against the state-specific correction, that is, the difference between PTED(cLR) and PTED(LR). For the $n\pi^*$ transition, the two contributions add up and increase in this case the discrepancy with the experimental result, probably because of the neglect of other contributions (London dispersion, Pauli repulsion) with a net effect in the opposite direction.

CONCLUSION

The current work presents the first systematic comparison of the post-SCF reaction field scheme with the PTE, PTED(LR), and PTED(cLR) schemes for vertical excitation energies under nonequilibrium conditions of molecular systems in solution

https://dx.doi.org/10.1021/acs.jctc.0c00316
J. Chem. Theory Comput. 2020, 16, 4554−4564

with a correlated wave function method, ADC(2), and a continuum solvation model (COSMO). The study is motivated by problems that excited-state specific corrections, for example, for the cLR approach cause for potential energy surfaces and the high computational costs of the PTED schemes. These problems have been demonstrated for excited-state potential energy curves of DMABN along the phenyl-amino torsion angle. The behavior of the PES obtained with the LR and cLR approaches is in particular important in the regions of avoided crossings. The post-SCF scheme, which includes the LR contributions approach, was recently used in our implementation of COSMO-ADC(2) for vertical excitation energies, UV/vis and magnetic circular dichroism spectra,[20,68,69] and analytic excited-state gradients. It gives physically correct results for potential energy surfaces especially at the avoided crossings while the perturbative addition of the state-specific contribution in cLR approaches, like the PTED(cLR) scheme used here, introduce artifacts which lead to an unphysical behavior in these regions.

The respective performance of these reaction field schemes for predicting solvatochromic shifts in absorption spectra was examined for two different data sets. The first one was taken from Mewes et al.[22] and focuses on the solvatochromism of molecules with $\pi\pi^*$ transitions, mostly nitrobenzene derivatives, in nonprotic solvents and a second new complementary data set which is composed of more diverse molecular structures with both $\pi\pi^*$ and $n\pi^*$ transitions in nonprotic and protic solvents.

For data set I, as expected, solvent shifts for less polar solvents like cyHex are generally smaller than for more polar ones, for example, Et_2O and MeCN. We observed that for this test set the COSMO-ADC(2) as QM method with the post-SCF scheme provides somewhat more accurate solvent shifts than PTED(cLR) at less computational cost. These approaches perform better than the PTE scheme.

For data set II, the post-SCF scheme performs for $n\pi^*$ states closely to PTED(LR) and slightly better than PTED(cLR) and for $\pi\pi^*$ transitions it shows about the same performance as PTED(cLR) in comparison with the experimental solvent shifts. For both data sets, the post-SCF and PTED RF schemes give significantly more accurate results than the PTE scheme. Thus, generally, for calculations at the COSMO-ADC(2) level, the PTE scheme is not a preferable approach due to the complete neglect of the coupling between the RF and the transition density. However, of the PTED and the post-SCF approaches, which include the coupling of the transition density to the reaction field and give in general results of similar accuracy, the post-SCF scheme produces more accurate results for test set I, which is dominated by transitions in nitrobenzenes with significant charge-transfer contributions and has significantly lower computational costs. For both test sets, the results of the perturbative state-specific correction added in the cLR approach to the LR does not improve the agreement between computation and experiment. For continuum solvation models, which account implicitly for the sampling over solvent configurations, the computed vertical excitation energies can only be tested against experiment for band maxima. Such a comparison has an intrinsic uncertainty that might be in the order of a few hundredth eV and hinders the separation of errors due to the reaction field scheme from those due to the electronic structure method. This makes it difficult to tell if the perturbative state-specific correction does not improve the results because it is itself inaccurate or because its inclusion destroys a fortuitous error cancellation. This question can possibly be resolved by a comparison between atomistic QM/MM-like polarizable embedding and supermolecular calculations[70] that treat the whole system at the same level of theory that exclude these problems. But this is beyond the scope of the current paper, where we tried to shed some light on the performance of different reaction field scheme for the combination of correlated wave function methods with continuum solvation models.

From the results obtained in this work, we conclude that the sum of the state-specific correction for the cLR approach and the additional correlation effects that are included in the PTED but not in the post-SCF scheme is small and in most cases negligible relative to the errors caused by the nonelectrostatic contributions (e.g., London dispersion and Pauli repulsion), the intrinsic errors of continuum solvation models and the comparison between computed solvent shifts on vertical excitation energies and experimental shifts of band maxima.

■ ASSOCIATED CONTENT

Supporting Information

The Supporting Information is available free of charge at https://pubs.acs.org/doi/10.1021/acs.jctc.0c00316.

Detailed information about MD simulation of pyridazine and the subsequent H-bond analysis and experimental and computational values for excitation energies in vacuum and solution (PDF)

■ AUTHOR INFORMATION

Corresponding Author

Sarah Karbalaei Khani − *Arbeitsgruppe Quantenchemie, Ruhr-Universität, Bochum 44780, Germany;* orcid.org/0000-0002-7366-2916; Email: Sarah.Karbalaeikhani@ruhr-uni-bochum.de

Authors

Alireza Marefat Khah − *Arbeitsgruppe Quantenchemie, Ruhr-Universität, Bochum 44780, Germany;* orcid.org/0000-0002-9593-0344

Christof Hättig − *Arbeitsgruppe Quantenchemie, Ruhr-Universität, Bochum 44780, Germany;* orcid.org/0000-0002-5752-2710

Complete contact information is available at: https://pubs.acs.org/10.1021/acs.jctc.0c00316

Notes

The authors declare no competing financial interest.

■ ACKNOWLEDGMENTS

We acknowledge financial support by the Deutsche Forschungsgemeinschaft through project Ha 2588/8-1. Funded by the Deutsche Forschungsgemeinschaft (DFG, German Research Foundation) under Germany's Excellence Strategy—EXC 2033—390677874—RESOLV.

■ REFERENCES

(1) Watanabe, H. C.; Cui, Q. Quantitative Analysis of QM/MM Boundary Artifacts and Correction in Adaptive QM/MM Simulations. *J. Chem. Theory Comput.* **2019**, *15*, 3917−3928.

(2) Kloss, T.; Heil, J.; Kast, S. M. Quantum Chemistry in Solution by Combining 3D Integral Equation Theory with a Cluster Embedding Approach. *J. Phys. Chem. B* **2008**, *112*, 4337−4343.

(3) Weijo, V.; Mennucci, B.; Frediani, L. Toward a General Formulation of Dispersion Effects for Solvation Continuum Models. *J. Chem. Theory Comput.* **2010**, *6*, 3358−3364.
(4) Miertuš, S.; Scrocco, E.; Tomasi, J. Electrostatic interaction of a solute with a continuum. A direct utilization of *ab initio* molecular potentials for the prevision of solvent effects. *Chem. Phys.* **1981**, *55*, 117−129.
(5) Cancès, E.; Mennucci, B.; Tomasi, J. A new integral equation formalism for the polarizable continuum model: theoretical background and applications to isotropic and anisotropic dielectrics. *J. Chem. Phys.* **1997**, *107*, 3032−3041.
(6) Barone, V.; Cossi, M. Quantum calculation of molecular energies and energy gradients in solution by a conductor solvent model. *J. Phys. Chem. A* **1998**, *102*, 1995−2001.
(7) Klamt, A.; Schüürmann, G. COSMO: A new approach to dielectric screening in solvents with explicit expressions. *J. Chem. Soc., Perkin Trans. 2* **1993**, 799−805.
(8) Cramer, C. J.; Truhlar, D. G. Implicit solvation models: equilibria, structure, spectra and dynamics. *Chem. Rev.* **1999**, *99*, 2161−2200.
(9) Cammi, R.; Corni, S.; Mennucci, B.; Tomasi, J. Electronic excitation energies of molecules in solution: State specific and linear response methods for nonequilibrium continuum solvation models. *J. Chem. Phys.* **2005**, *122*, 104513−1−12.
(10) Corni, S.; Cammi, R.; Mennucci, B.; Tomasi, J. Electronic excitation energies of molecules in solution within continuum solvation models: Investigating the discrepancy between state-specific and linear-response methods. *J. Chem. Phys.* **2005**, *123*, 134512−1−10.
(11) Canuto, S.; Coutinho, K.; Zerner, M. C. Including dispersion in configuration interaction-singles calculations for the spectroscopy of chromophores in solution. *J. Chem. Phys.* **2000**, *112*, 7293−7299.
(12) Lunkenheimer, B.; Köhn, A. Solvent effects on electronically excited states using the conductor-like screening model and the second-order correlated method ADC(2). *J. Chem. Theory Comput.* **2013**, *9*, 977−994.
(13) Caricato, M.; Mennucci, B.; Tomasi, J.; Ingrosso, F.; Cammi, R.; Corni, S.; Scalmani, G. Formation and relaxation of excited states in solution: A new time dependent polarizable continuum model based on time dependent density functional theory. *J. Chem. Phys.* **2006**, *124*, 124520.
(14) Jacquemin, D.; Wathelet, V.; Perpete, E. A.; Adamo, C. Extensive TD-DFT Benchmark: Singlet-Excited States of Organic Molecules. *J. Chem. Theory Comput.* **2009**, *5*, 2420−2435.
(15) Laurent, A. D.; Jacquemin, D. TD-DFT benchmarks: A review. *Int. J. Quantum Chem.* **2013**, *113*, 2019−2039.
(16) Jacquemin, D.; Duchemin, I.; Blase, X. 0−0 Energies Using Hybrid Schemes: Benchmarks of TD-DFT, CIS(D), ADC(2), CC2, and BSE/GWformalisms for 80 Real-Life Compounds. *J. Chem. Theory Comput.* **2015**, *11*, 5340−5359.
(17) del Valle, F. J. O.; Tomasi, J. Electron correlation and solvation effects. I. Basic formulation and preliminary attempt to include the electron correlation in the quantum mechanical polarizable continuum model so as to study solvation phenomena. *Chem. Phys.* **1991**, *150*, 139−150.
(18) Caricato, M. CCSD-PCM: Improving upon the reference reaction field approximation at no cost. *J. Chem. Phys.* **2011**, *135*, 074113−1−7.
(19) Schwabe, T.; Sneskov, K.; Haugaard Olsen, J. M.; Kongsted, J.; Christiansen, O.; Hättig, C. PERI-CC2: A polarizable embedded RI-CC2 method. *J. Chem. Theory Comput.* **2012**, *8*, 3274−3283.
(20) Karbalaei Khani, S.; Marefat Khah, A.; Hättig, C. COSMO-RI-ADC(2) excitation energies and excited state gradients. *Phys. Chem. Chem. Phys.* **2018**, *20*, 16354−16363.
(21) Marefat Khah, A.; Karbalaei Khani, S.; Hättig, C. Analytic excited state gradients for the QM/MM polarizable embedded second−order algebraic diagrammatic construction for the polarization propagator PE-ADC(2). *J. Chem. Theory Comput.* **2018**, *14*, 4640−4650.
(22) Mewes, J. M.; You, Z. Q.; Wormit, M.; Kriesche, T.; Herbert, J. M.; Dreuw, A. Experimental benchmark data and systematic evaluation of two a posteriori, polarizable-continuum corrections for vertical excitation energies in solution. *J. Phys. Chem. A* **2015**, *119*, 5446−5464.
(23) Klamt, A.; Diedenhofen, M. A refined cavity construction algorithm for the conductor-like screening model. *J. Comput. Chem.* **2018**, *39*, 1648−1655.
(24) Ángyán, J. G. Choosing between alternative MP2 algorithms in the self-consistent reaction field theory of solvent effects. *Chem. Phys. Lett.* **1995**, *241*, 51−56.
(25) Corni, S.; Cammi, R.; Mennucci, B.; Tomasi, J. Electronic excitation energies of molecules in solution within continuum solvation models: Investigating the discrepancy between state-specific and linear-response methods. *J. Chem. Phys.* **2005**, *123*, 134512.
(26) Hättig, C. Structure optimization for excited states with correlated second-order methods: CC2, CIS(D_∞) and ADC(2). *Adv. Quantum Chem.* **2005**, *50*, 37−60.
(27) Mennucci, B.; Cammi, R., Eds. *Continuum Solvation Models in Chemical Physics*; John Wiley & Sons, Ltd., 2007.
(28) Mennucci, B.; Cappelli, C.; Guido, C. A.; Cammi, R.; Tomasi, J. Structures and Properties of Electronically Excited Chromophores in Solution from the Polarizable Continuum Model Coupled to the Time-Dependent Density Functional Theory. *J. Phys. Chem. A* **2009**, *113*, 3009−3020.
(29) Weigend, F.; Ahlrichs, R. Balanced basis sets of split valence, triple zeta valence and quadruple zeta valence quality for H to Rn: Design and assessment of accuracy. *Phys. Chem. Chem. Phys.* **2005**, *7*, 3297−3305.
(30) Millefiori, S.; Zuccarello, F.; Buemi, G. Excited state dipole moments of nitrobenzene derivatives. *J. Chem. Soc., Perkin Trans. 2* **1978**, 849−852.
(31) Buemi, G.; Millefiori, S.; Zuccarello, F.; Millefiori, A. Excited state properties of nitrobenzene derivatives. *Can. J. Chem.* **1979**, *57*, 2167−2171.
(32) Moskvin, A. F.; Yablonskii, O. P.; Bondar, L. F. An experimental investigation of the effect of alkyl substituents on the position of the K and R absorption bands in acrolein derivatives. *Theor. Exp. Chem.* **1968**, *2*, 469−472.
(33) Inuzuka, K. Near ultraviolet absorption spectra of acrolein and crotonaldehyde. *Bull. Chem. Soc. Jpn.* **1960**, *33*, 678−680.
(34) Hollas, J. M. The electronic absorption spectrum of acrolein vapour. *Spectrochim. Acta* **1963**, *19*, 1425−1441.
(35) Aidas, K.; Møgelhøj, A.; Nilsson, E. J. K.; Johnson, M. S.; Mikkelsen, K. V.; Söderhjelm, O. C. P.; Kongsted, J.; et al. On the performance of quantum chemical methods to predict solvatochromic effects: The case of acrolein in aqueous solution. *J. Chem. Phys.* **2008**, *128*, 194503.
(36) Moskvin, A. F.; Yablonskii, O. P.; Bondar, L. F. *Theor. Exp. Chem.* **1966**, *2*, 636.
(37) Andersson, J.; Petterson, R.; Tegner, L. Flash photolysis experiments in the vapour phase at elevated temperatures I: Spectra of azobenzene and the kinetics of its thermal cis-trans isomerization. *J. Photochem.* **1982**, *20*, 17−32.
(38) Lednev, I.; Ye, T.; Matousek, P.; Towrie, M.; Foggi, P.; Neuwahl, F.; Umapathy, S.; Hester, R.; Moore, J. Femtosecond time-resolved UV-visible absorption spectroscopy of trans-azobenzene: dependence on excitation wavelength. *Chem. Phys. Lett.* **1998**, *290*, 68−74.
(39) Ohmori, N.; Suzuki, T.; Ito, M. Why does intersystem crossing occur in isolated molecules of benzaldehyde, acetophenone and benzophenone. *J. Phys. Chem.* **1988**, *92*, 1086−1093.
(40) Molina, V.; Merchán, M. Theoretical analysis of the electronic spectra of benzaldehyde. *J. Phys. Chem. A* **2001**, *105*, 3745−3751.
(41) Nakashima, K.; Koyanagi, M. Solvent intensification effects on the $S_{1(n\pi^*)} \leftarrow S_0$ absorption spectra of benzaldehyde in fluid solutions. *Bull. Chem. Soc. Jpn.* **1982**, *55*, 3923−3924.
(42) Georgieva, I.; Aquino, A. J. A.; Plasser, F.; Trendafilova, N.; Köhn, A.; Lischka, H. Intramolecular charge-transfer excited-state

https://dx.doi.org/10.1021/acs.jctc.0c00316
J. Chem. Theory Comput. 2020, 16, 4554−4564

processes in 4-(N,N-Dimethylamino)benzonitrile: The role of twisting and the $\pi\sigma^*$ state. *J. Phys. Chem. A* **2015**, *119*, 6232−6243.
(43) Zachariasse, K. A.; Grobys, M.; Tauer, E. Absence of dual fluorescence with 4-(dimethylamino)phenylacetylene. A comparison between experimental results and theoretical predictions. *Chem. Phys. Lett.* **1997**, *274*, 372−382.
(44) Galievsky, V. A.; Zachariasse, K. A. Intramolecular charge transfer with N,N,-Dialkyl-4-(Trfluoromethyl)anilines and 4-(Dimethylamino)benzonitrile in polar solvents. Investigation of the excitation wavelength dependence of the reaction pathway. *Acta Phys. Pol., A* **2007**, *112*, S39−S56.
(45) Castle, R. N. *Pyridazines*; John Wiley & Sons, 1973.
(46) Fraser, J. R.; Low, L. H.; Weir, N. A. Photolysis of pyridazine in the gas phase. *Can. J. Chem.* **1975**, *53*, 1456−1460.
(47) Parkin, J. E.; Innes, K. K. The vacuum ultraviolet spectra of pyrazine, pyrimidine and pyridazine vapors. *J. Mol. Spectrosc.* **1965**, *15*, 407−434.
(48) Parac, M.; Grimme, S. Comparison of multireference Møller-Plesset Theory and Time-Dependent methods for the calculation of vertical excitation energies of molecules. *J. Phys. Chem. A* **2002**, *106*, 6844−6850.
(49) Halverson, F. c; Hirt, R. The near ultraviolet absorption spectra of the diazines. *J. Chem. Phys.* **1949**, *17*, 1165−1166.
(50) Halverson, F. c.; Hirt, R. Near ultraviolet solution spectra of the diazines. *J. Chem. Phys.* **1951**, *19*, 711−718.
(51) Lambert, W. R.; Felker, P. M.; Syage, J. A.; Zewail, A. H. Jet spectroscopy of anthracene and deuterated anthracenes. *J. Chem. Phys.* **1984**, *81*, 2195−2208.
(52) Jones, R. N. *Chem. Rev.* **1947**, *41*, 353−371.
(53) Li, L.; Lubman, D. M. Ultraviolet-visible absorption spectra of biological molecules in the gas phase using pulsed laser-induced volatilization enhancement in a diode array spectrophotometer. *Anal. Chem.* **1987**, *59*, 2538−2541.
(54) Barbatti, M.; Aquino, A. J. A.; Lischka, H. The UV absorption of nucleobases: semi-classical ab initio spectra simulations. *Phys. Chem. Chem. Phys.* **2010**, *12*, 4959−4967.
(55) Clark, L. B.; Peschel, G. G.; Tinoco, I. Vapor spectra and heats of vaporization of some purine and pyrimidine bases. *J. Phys. Chem.* **1965**, *69*, 3615−3618.
(56) Middleton, C. T.; de La Harpe, K.; Su, C.; Law, Y. K.; Crespo-Hernández, C. E.; Kohler, B. DNA excited-state dynamics: From single bases to the double Helix. *Annu. Rev. Phys. Chem.* **2009**, *60*, 217−239.
(57) Hollas, J. M. Vapour-phase ultra-violet absorption spectra of indene, indole, coumarone and thionaphthene. *Spectrochim. Acta* **1963**, *19*, 753−767.
(58) Serrano-Andrés, L.; Roos, B. O. Theoretical study of the absorption and emission spectra of indole in the gas phase and in a solvent. *J. Am. Chem. Soc.* **1996**, *118*, 185−195.
(59) Lalevee, J.; Blanchard, N.; Tehfe, M. A.; Fries, C.; Morlet-Savary, F.; Gigmes, D.; Fouassier, J. P. New thioxanthone and xanthone photoinitiators based on silyl radical chemistry. *Polym. Chem.* **2011**, *2*, 1077−1084.
(60) Cavaleri, J. J.; Prater, K.; Bowman, R. M. An investigation of the solvent dependence on the ultrafast intersystem crossing kinetics of xanthone. *Chem. Phys. Lett.* **1996**, *259*, 495−502.
(61) Bayliss, N. S.; McRae, E. G. Solvent effects in the spectra of acetone, crotonaldehyde, nitromethane and nitrobenzene. *J. Phys. Chem.* **1954**, *58*, 1006−1011.
(62) *TURBOMOLE*, v 7.3; TURBOMOLE GmbH, 2018. http://www.turbomole.com.
(63) Hellweg, A.; Hättig, C.; Höfener, S.; Klopper, W. Optimized accurate auxiliary basis sets for RI-MP2 and RI-CC2 calculations for the atoms Rb to Rn. *Theor. Chem. Acc.* **2007**, *117*, 587−597.
(64) Furche, F.; Ahlrichs, R.; Hättig, C.; Klopper, W.; Sierka, M.; Weigend, F. *Wiley Interdiscip. Rev.: Comput. Mol. Sci.* **2014**, *4*, 91−100.
(65) Klamt, A.; Jonas, V.; Bürger, T.; Lohrenz, J. C. W. Refinement and Parametrization of COSMO-RS. *J. Phys. Chem. A* **1998**, *102*, 5074−5085.
(66) Schäfer, A.; Klamt, A.; Sattel, D.; Lohrenz, J. C. W.; Eckert, F. COSMO Implementation in TURBOMOLE: Extension of an efficient quantum chemical code towards liquid systems. *Phys. Chem. Chem. Phys.* **2000**, *2*, 2187−2193.
(67) Best, R. B.; Zhu, X.; Shim, J.; Lopes, P. E. M.; Mittal, J.; Feig, M.; MacKerell, A. D. Optimization of the Additive CHARMM All-Atom Protein Force Field Targeting Improved Sampling of the Backbone Φ, Ψ and Side-Chain X(1) and X(2) Dihedral Angles. *J. Chem. Theory Comput.* **2012**, *8*, 3257−3273.
(68) Karbalaei Khani, S.; Faber, R.; Santoro, F.; Coriani, S.; Hättig, C. UV Absorption and Magnetic Circular Dichroism Spectra of Purine, Adenine, and Guanine: A Coupled Cluster Study in Vacuo and in Aqueous Solution. *J. Chem. Theory Comput.* **2019**, *15*, 1242−1254.
(69) Coriani, S.; Jørgensen, P.; Rizzo, A.; Ruud, K.; Olsen, J. Ab initio determinations of magnetic circular dichroism. *Chem. Phys. Lett.* **1999**, *300*, 61−68.
(70) Marefat Khah, A.; Reinholdt, P.; Olsen, J. M. H.; Kongsted, J.; Hattig, C. Avoiding Electron Spill-Out in QM/MM Calculations on Excited States with Simple Pseudopotentials. *J. Chem. Theory Comput.* **2020**, *16*, 1373−1381.

https://dx.doi.org/10.1021/acs.jctc.0c00316
J. Chem. Theory Comput. 2020, 16, 4554−4564